Ultrasonics Sonochemistry 89 (2022) 106119

Contents lists available at ScienceDirect

Ultrasonics Sonochemistry

journal homepage: www.elsevier.com/locate/ultson

Numerical study of the synergistic effect of cavitation and micro-abrasive particles

Yingze Fu [a,b], Xijing Zhu [a,b,*], Jianqing Wang [a,b], Tai Gong [a,b]

[a] Shanxi Key Laboratory of Advanced Manufacturing Technology, North University of China, Taiyuan, Shanxi 030051, China
[b] School of Mechanical Engineering, North University of China, Taiyuan, Shanxi 030051, China

ARTICLE INFO

Keywords:
Ultrasonic cavitation
Micro-jet
Shock wave
Micro-abrasive particle
Velocity
Pressure

ABSTRACT

In ultrasonic-assisted machining, the synergistic effect of the cavitation effect and micro-abrasive particles plays a crucial role. Studies have focused on the investigation of the micro-abrasive particles, cavitation micro-jets, and cavitation shock waves either individually or in pairs. To investigate the synergy of shock waves and micro-jets generated by cavitation with micro-abrasive particles in ultrasonic-assisted machining, the continuous control equations of a cavitation bubble, shock wave, micro-jet, and micro-abrasive particle influenced by the dimensionless amount (R/R_0), a particle size-velocity–pressure model of the micro-abrasive particle was established. The effects of ultrasonic frequency, sound pressure amplitude, and changes in particle size on micro-abrasive particle velocity and pressure were numerically simulated. At an ultrasonic frequency of 20 kHz and ultrasonic sound pressure of 0.1125 MPa, a smooth spherical SiO_2 micro-abrasive particle (size = 5 μm) was obtained, with a maximum velocity of 190.3–209.4 m/s and pressure of 79.69–89.41 MPa. The results show that in the range of 5–50 μm, smaller particle sizes of the micro-abrasive particles led to greater velocity and pressure. The shock waves, micro-jets, and micro-abrasive particles were all positively affected by the dimensionless amount (R/R_0) of cavitation bubble collapse, the larger the dimensionless quantity, the faster their velocity and the higher their pressure.

1. Introduction

In ultrasonic cavitation, cavitation bubbles form, grow and implode and collapse in a liquid medium driven by ultrasonic pressure waves [1,2]. When cavitation bubbles have no boundary and pressure gradient in the growth space, they maintain spherical symmetry. Shock waves, the micro-abrasive particles in a medium, and pressure gradient caused by gravity are some of the factors that cause cavitation bubbles to collapse asymmetrically [3], and this generates micro-jets [4]. Therefore, the collapse of cavitation bubbles is mainly asymmetric collapse, and it is accompanied by the generation of shock waves and micro-jets (i.e., the cavitation effect). In the past few decades, there has been extensive experimental and theoretical research on the individual behaviors of shock waves, micro-jets, and micro-abrasive particles, as well as in pairs, however, it is still necessary to study the three interactions as a whole and establish a more accurate quantitative model.

Ultrasonic-assisted machining technology combines traditional and ultrasonic machining, it demonstrates the practical application of the ultrasonic cavitation effect based on traditional machining. Ultrasonic vibration-assisted processing is used on structured surfaces with complex micro/nanostructures [5,6]. Chen et al. [7] conducted a vibration cavitation erosion test of 40Cr steel; they determined that complete and incomplete corrosion pits are attributed to large-radius micro-jet flows and shock waves generated outside the action distance of the micro-jet, respectively. The interpretation of the pits [8] can deepen our understanding of the shape and pressure of the effect of cavitation shock waves and micro-jets on the surface of a machined workpiece. A complete understanding of the cavitation effect can highlight its more effective role in practical applications.

There has been extensive research on ultrasonic cavitation shock waves [9,10]and micro-jets. In 1944, Kornfeld [11] first proposed the theory of micro-jets. Ye and Zhu [12] conducted ultrasonic cavitation tests and inversion analyses to explore the influence of near-wall acoustic cavitation collapse micro-jets on a 1060 aluminum plate. The results showed that when the indent-depth ratio of micro-jet impact was 16–68, the impact strength of the micro-jet was 420–500 MPa, and the corresponding velocity of the micro-jet was 310–370 m/s. Tzanakis [39] carried out cavitation impact tests on steel samples using an ultrasonic

* Corresponding author at: School of Mechanical Engineering, North University of China, Taiyuan, Shanxi 030051, China.
E-mail address: zxj161501@163.com (X. Zhu).

https://doi.org/10.1016/j.ultsonch.2022.106119
Received 12 June 2022; Received in revised form 25 July 2022; Accepted 5 August 2022
Available online 8 August 2022

transducer with a probe diameter of 5 mm, they usd a reverse engineering approach to determine that jet impingement was in the range of 0.4–1 GPa, with corresponding jet velocities of 200–700 m/s. Table 3 lists the results of several studies on micro-jet pressure and velocity obtained via various methods, which include experiments and numerical simulations; it provides a reference for further accurate quantification of both micro-jets.

In addition to micro-jets, shock waves are an important component of the cavitation effect. During the collapse of a bubble, strong shock waves are generated and propagate through the liquid at speeds higher than the speed of sound. Many researchers have presented methods for quantifying and understanding shock waves through experimental measurements. In the 1980 s and 1990 s, Field [13,14] and others used a combination of ripple shadowing and high-speed photography to study the interaction between the shock wave generated by an impact shocker and a stationary bubble in a two-dimensional gelatin gel; and observed that the shock wave caused the bubble to collapse under the action of a micro-jet in the direction in which the shock wave was that traveling. Although the bubbles in Field's experiments were not generated by ultrasound at the time, the findings are still relevant for experimental studies of shock waves and bubbles. Several researchers have also corroborated the accuracy of Field's results; Klaseboer [15] demonstrated that shock waves cause bubbles to collapse, producing micro-jets that follow the direction of the shock wave. Petkovšek et al.[16] used visualization to show that the collapse of a cavitation cloud in a large volume of liquid generates a full range of shock waves; they estimated the shock wavefront velocity and local pressure wave caused by bubble cloud collapse were $>$ 700 m/s and 5 MPa, respectively. Brujan [20] investigated shock waves via ultrasonically generated cavitation bubble collapse; shock wave velocities and pressures were experimentally determined to be 1500–2520 m/s and 1.3 $\pm$ 0.3 GPa, respectively; Table 2 lists results of previous studies of cavitation shock wave velocities and pressures. Khavari et al. [17] measured the shock wave pressure generated by a cavitating bubble in water excited by an ultrasonic probe at 24 kHz and obtained a consistent resonance peak in a very narrow frequency range (3.27–3.43 MHz); this new peak may be attributed r to the shock waves emission from the ruptured bubble, as verified by obtaining that the shock wave attenuates along the symmetry axis and is stronger at the edges.

Shock waves are generated at ultrasonic speeds, and they decay instantly by losing energy rapidly [18]. The decay rate of shock waves has been experimentally investigated by several researchers; decay rates have been determined to be $1/r$ [19], $1/r^{1.5}$[20], $1/r^{2.3}$[21], and so on. Khavari [17] observed a 97–98 % decrease in the maximum pressure of shock waves for three different input power transducers at a distance of 10 mm; Vogel, Busch & Parlitz [22] also confirmed that the mechanical energy of shock waves is significantly dissipated within the first 10 mm of propagation. Thus, shock waves are generated and dissipated rapidly, which explains why they cannot be observed by the naked eye.

Ultrasonically assisted machining with the addition of micro-abrasive particles can effective enhance the efficiency and improve the surface quality of ultrasonic polishing of advanced materials with high strength, hardness, and brittleness [1]. Soh et al.[23] indicated that the addition of particles to the cavitation stream can produce effects far beyond the cavitation effect alone or the particle effect alone. Zhang et al. [24] proposed the concept of a suspension with a sufficiently small gap infiltrated between the polishing tool and the machined workpiece as a suspension film (STF) and used ultrasonic polishing (USP) experiments and computational fluid dynamics (CFD) simulations to form a strong transverse shear flow in the STF, which is crucial for material removal. The finite element method (FEM) was also used to investigate the effects of abrasive particle size, kinetic energy change, impact force analysis, and impact angle on the material removal rate. Bifano et al. [25], in their study on the processing of brittle materials, found that hard brittle materials also have properties similar to plastic deformation of plastic materials. Peng et al. [26] performed ultrasonic cavitation erosion of reservoir rocks in distilled water containing SiO_2 and without SiO_2, respectively; they showed that the presence of micro-abrasives increases the ultrasonic cavitation erosion of the reservoir rocks, and the synergistic effect with cavitation promotes the erosion of the workpiece surface. Thus, adding micro-abrasives to the ultrasonically assisted process positively influences the material surface.

Contemporary studies have focused on the interaction between individual bubbles and single abrasive particles; they determined that the collapse of a bubble accelerates the motion of abrasive particles, but with varying ways of the acceleration mechanism. In this study, we present that before the collapse of a bubble, the bubble itself does not have an acceleration mechanism in the absence of cavitation nucleation; rather, the collapse of the bubble generates a shock wave and a micro-jet, both of which act together at high transient pressures on the micro-abrasive grain, and the sudden impact of both is the source of acceleration. Both have an accelerating effect on the motion of micro-abrasive particles, and they also cause particle breakage. Zhang et al. [27] showed that during bubble rupture, micro-jets, shock waves, and high-speed inter-particle collisions lead to effective local deformation of the surfaces of micro-abrasive particles; these deformations are mainly caused by interactions between particles and shock waves. The critical effect of the initial size of a solid particle on the internal fracture of the particle under ultrasound was predicted, and the following results were obtained: SiO_2 particles ($<$2 μm) are unlikely to rupture with sufficient energy to collide. Prozorov et al. [28] found that shock waves cause high-speed collisions between micro-abrasive particles and that the initial size of the solid particles critically influences inter-particle collisions. In the case of zinc, for example, particles smaller than a few microns or larger than a few tens of microns will not collide with sufficient energy to aggregate. Irrespective of the size of the micro-abrasive particles, the micro-jets and shock waves cause the micro-abrasive particles in the liquid medium to acquire a certain velocity, and this velocity has a micro-cutting effect on the surface of the machined workpiece.

As seen in the above discussions, several researchers have investigated micro-abrasive particles, cavitation micro-jets, and cavitation shock waves either individually or in pairs; however, it is relatively rare to see all three studied together. In this study, theoretical analyses and numerical simulations based on the basic equations of cavitation bubble dynamics, cavitation micro-jet control equation, cavitation shock wave control equation, and Newtonian mechanics velocity equation of micro-abrasive particle are used to obtain the velocity and pressure of shock wave, micro-jet, and the micro-abrasive particle, respectively. This provides insights for investigating the three together. Most previous studies have been based on the inversion analysis of micro-abrasive particle velocity through the mass loss of the workpiece. However, in this study, the velocity and pressure model of micro-abrasive particles is directly established, which provides a reference for the selection of ultrasonic parameters and micro-abrasive particle parameters in ultrasonic machining and reduces the cost of trial and error.

2. Methods

First, cavitation bubbles, micro-jets, shock waves, and the micro-abrasive particles are modeled simultaneously. The dimensionless

Table 1
Values of relevant model parameters.

P_a/Pa	f/Hz	c/(m/s)	ρ/(kg/m^3)	μ/(Pa·s)	R_0(m)	P_v/Pa	σ(N/m)	ξ	γ
101,300	20,000	1500	998	0.001	5×10^{-6}	2330	0.0725	100	3/4

Table 2
Examples of shock wave velocities and pressures.

Literature	Cavitation source	Method of derivation	Shock wave velocity	Shock wave pressure
Mozina&Mocnik [21]	Laser-induced	Experiment&numerical	Up to 2700 m/s	>1 GPa
Pecha [19]	Laser-induced	Experiment	Up to 4000 m/s	40–60 kbar
Brujan [20]	Ultrasound	Experiment	1500–2520 m/s	1.3 ± 0.3 GPa
Holzfuss [38]	Ultrasound	Numerical	1500–5500 m/s	Up to 1 GPa
Petkovsek [16]	Ultrasound	Experiment	700 m/s	5 MPa

Table 3
Examples of micro-jet velocities and pressures.

Literature	Cavitation source	Method of derivation	Micro-jet velocity	Micro-jet pressure
Tzanakis [39]	Ultrasound (20 kHz)	Experiment&HSC	200–700 m/s	0.4–1 GPa
Linzheng [40]	Ultrasound (20 kHz)	Numerical	355–848 m/s	273–1131 MPa
Pishchalnikov [41]	Ultrasound (20 kHz)	Numerical&HSC	Up to 1164 m/s	Up to 0.65 GPa
Petkovsek, R [42]	Laser-induced	Numerical&BDP scanning	300 ~ 780 m/s	—
Chen, H.S [43]	Ultrasound (20 kHz)	Experiment	200–1300 m/s	264–1761 MPa

amount (R/R_0) affects each model, and the interaction between the models is obtained through numerical analysis.

The generally accepted shock wave and micro-jet generation process [29] is that the shock wave generated by the cavitation cloud contacts the cavitation bubble near the wall, resulting in different pressures up to and below the spherical cavitation bubble; the bubble collapses and releases energy to generate micro-jets. Concurrently, generated shock waves and micro-jets [30] are the sources of micro-abrasive acceleration. Fig. 1(a) provides an intuitive understanding of the relationship between the three; Fig. 1(b) shows the forces on the micro-abrasive particle grains as they move.

2.1. Mathematical model of cavitation bubble dynamics

Common models used for cavitation bubble dynamics are the Rayleigh-Plesset model (R-P model) [31], Gilmore model [32], and Keller-Miksis model (K-M model) [33]. For two compressible fluid models, the Gilmore equation is suitable for describing high Mach numbers [34] and investigating large-amplitude acoustic cavitation at high driving sound pressures. The modified K-M equation applies to vibrations of various amplitudes and produces results that agree well with those obtained by solving the full partial differential equations of fluid dynamics. Therefore, we selected the modified Keller-Miksis model (Eq. (1)) in this study [33]:

$$\left(1-\frac{\dot{R}}{c}\right)R\ddot{R}+\frac{3}{2}\dot{R}^2\left(1-\frac{\dot{R}}{3c}\right)=\frac{P}{\rho}+\frac{1}{\rho c}\frac{d}{dt}(RP)=\left(1+\frac{\dot{R}}{c}\right)\frac{P}{\rho}+\frac{R}{\rho c}\frac{dP}{dt} \tag{1}$$

According to the analysis of internal and external forces of the cavitation bubble wall, the pressure, P, of the liquid outside the cavitation bubble wall is given using Eq. (2) [33]:

$$P=\left(P_0-P_v+\frac{2\sigma}{R_0}\right)\left(\frac{R_0}{R}\right)^{3\gamma}-\frac{2\sigma}{R}-\frac{4\mu\dot{R}}{R}-P_0+P_v-P_a\sin(2\pi ft) \tag{2}$$

According to the conservation of energy, cavitation wall velocity is obtained using Eq. (3):

$$\dot{R}=\left\{\frac{2P_\infty}{3\rho}\left[\left(\frac{R_0}{R}\right)^3-1\right]+\frac{2\sigma}{\rho R_0}\left[\left(\frac{R_0}{R}\right)^3-\frac{R_0}{R}\right]-\frac{2P_0}{3(1-\gamma)}\left[\left(\frac{R_0}{R}\right)^{3(1-\lambda)}-1\right]\right\}^{\frac{1}{2}} \tag{3}$$

where P_a and f are the sound pressure amplitude and frequency, respectively, in the ultrasonic field. The parameters of liquid medium water appear in the formula; c is the normal sound velocity in water, ρ is the density of the liquid medium water, and μ is the viscosity of the liquid. There are also some parameters for the bubble itself; R_0 is the initial radius of a cavitation bubble, R is the radius of a cavitation bubble, and $\dot{R}$ and $\ddot{R}$ are the first and second derivatives of R with respect to time, t, respectively. P_v is the saturated vapor pressure in the cavitation bubble, σ is the surface tension coefficient, R_0 is the initial radius of the cavitation bubble, and γ is the polytropic index of the gas. The values of relevant model parameters are presented in Table 1.

The size of the bubble when it collapses is an index of the efficiency of converting ultrasonic energy into mechanical energy. The time-dependent curve of cavitation in the process of growth, development, and collapse is obtained by solving Eq. (1) through the fourth-order Runge-Kutta algorithm with Matlab, followed by extracting the dimensionless amount (R/R_0) of cavitation bubble collapse.

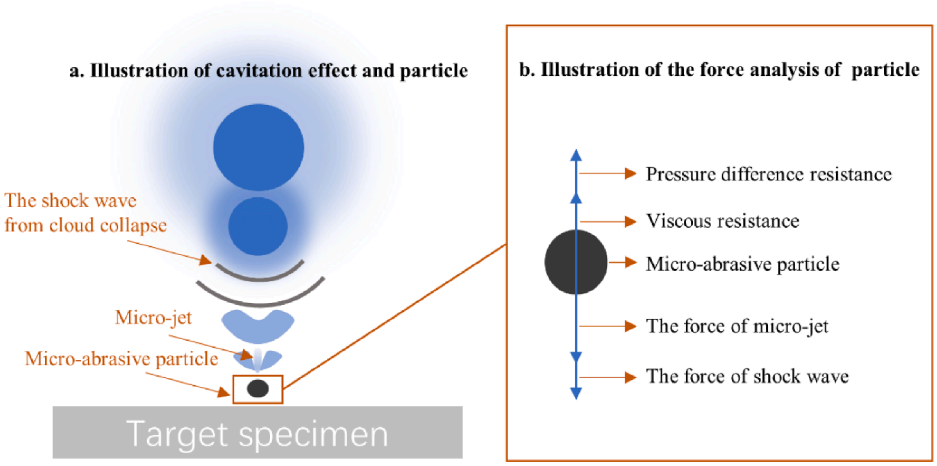

Fig. 1. Illustration of the interaction between cavitation effect and micro-abrasive particles.

2.2. Mathematical model of shock wave

We used the K-M model of cavitation bubble dynamics to obtain the dimensionless amount (R/R_0) of cavitation bubble collapse for calculating the velocity of the cavitation bubble wall. This is because we approximate bubble wall velocity during the collapse of a bubble as the velocity behind the shock front particles when the shock wave is emitted. The distance between the shock front and the bubble wall from the optical axis is plotted as a function of time by Vogel, A [9,10]. The shock wave pressure (P_s) was determined using Eq. (4):

$$P_s = c_1\rho u_s\left(10^{(u_s-c)/c_2}-1\right)+P_\infty \tag{4}$$

The particle velocity behind the shock front, u_p, was determined by Rice and Walsh [35] using Eq.5.

$$u_p = c_1\left(10^{\frac{(u_s-c)}{c_2}}-1\right) \tag{5}$$

According to the assumption that we approximate bubble wall velocity during the collapse of a bubble as the velocity behind the shock front particles when the shock wave is emitted, from (3) and (5), we get Eq. (6):

$$\dot{R} = u_p = c_1\left(10^{\frac{(u_s-c)}{c_2}}-1\right) \tag{6}$$

The values of u_s can be obtained using Eq. (6):

$$u_s = c + c_2\lg\left(\frac{\dot{R}}{c_1}+1\right) \tag{7}$$

where $c_1 = 5190$ m/s, $c_2 = 25306$ m/s, P_∞ is the environment pressure, $P_\infty = P_0 + P_a\sin(2\pi ft)$. To explore how well the results of the model match the experimental results, numerical analysis was also conducted.

2.3. Mathematical model of micro-jet

The shock wave hits the bubble, and micro-jets are generated in the same direction as the shock wave movement, as proven in several studies [36]. The process of cavitation bubble collapse to generate micro-jet is complex, rapid, microscopic, and random. Plesset and Chapmann presented the following micro-jet velocity (V_j) estimation formula (Eq. (8)) [37]:

$$V_j = 8.97\left(\frac{H}{R_0}\right)^2\sqrt{\frac{P_\infty - P_v}{\rho}} \tag{8}$$

where the new parameter H is the distance between the center of the bubble and the wall. In this paper, what we need is the initial velocity of the micro-jet, so H = R was obtained by considering the wall as the bubble wall.

The stage of the micro-jet impacting the workpiece surface was divided into the stage of water hammer pressure and stagnation pressure. Plesset and Chapmann [37] believed that water hammer pressure exerted by the micro-jet on the material is the main mechanism of solid surface damage. The water hammer pressure (P_j) is given using Eq. (9):

$$P_j \approx V_j\rho_0 c_0 \tag{9}$$

The velocity and pressure equations of micro-jets obtained so far were used to perform numerical analysis in Section 3.

2.4. Mathematical model of micro-abrasive particle

There has been extensive research interest in the acceleration mechanism of micro-abrasive particles due to cavitation bubble collapse. Microscopic interaction between cavitation and micro-abrasive particles has been explored in many experiments; however, few studies have established a strict numerical model depicting the physical interactions between the two. In this study, according to Newton's second law, we establish a numerical model of the velocity of micro-abrasive particles under the action of cavitation, providing a reference for the numerical modeling of the physical effects of the two.

According to the principle of mechanical vibration and Newton's second law, we get Eq. (10):

$$F_R - F_v - F_r = m\frac{dV_p}{dt} \tag{10}$$

where F_R is the resultant force of shock wave, micro-jet, and environmental pressure, F_V is the viscous resistance of the liquid, m is the mass of the single abrasive particle, and F_r is the pressure difference resistance. As the shock wave and the micro-jet are generated one after the other, the forces acting on the micro-abrasive particles are separated between the two. Therefore, we divide F_R into two types, shock wave action, F_{Rs}, and micro-jet action, F_{Rj} (Eqs. (11) and (12)):

$$F_{Rs} = F_s + F_\infty = (P_s + P_0 + P_a\sin(2\pi ft)) \times s \tag{11}$$

$$F_{Rj} = F_j + F_\infty = \left(P_j + P_0 + P_a\sin(2\pi ft)\right) \times s \tag{12}$$

where F_j, F_s, and F_∞ are the pressure of shock wave, micro-jet, and environmental, respectively, and s is the force area of the particle. The liquid viscous resistance is calculated using Eq. (13), which was obtained from Stokes formula ($r < 0.05$ mm):

$$F_v = 6\pi\mu r_p V_p \tag{13}$$

where r_p is the radius of a single-particle. The differential pressure resistance F_r during the movement of the micro-abrasive particle is:

$$F_s = \frac{1}{2}\xi\rho s V_p^2 \tag{14}$$

where ξ is the resistance coefficient. In the following equations, we use F_R instead of F_{Rs} and F_{Rj} for the time being, and then, we separate them when we simulate the numerical simulation in section 3. Based on Eqs. (10) to (14), we obtain the complete force equation for the particle as follows:

$$F_R - 6\pi\mu r_p V_p - \frac{1}{2}\xi\rho s V_p^2 = m\frac{dV_p}{dt} \tag{15}$$

According to the mathematical software Maple, we solve the nonlinear differential equation to obtain a general solution of micro-abrasive particle velocity (V_P):

$$V_P = \frac{1}{\xi\rho s}\left(-6\pi\mu r_p + \sqrt{(6\pi\mu r_p)^2 + 2F_R\xi\rho s}\tanh\left(\frac{1}{2m}(C + t)\sqrt{(6\pi\mu r_p)^2 + 2F_R\xi\rho s}\right)\right) \tag{16}$$

where C is a constant. When setting the initial condition $V_P(0) = 0$, we can solve to obtain C, so that the result for V_P is:

$$V_P = \frac{1}{\xi\rho s}\left(-6\pi\mu r_p + \sqrt{(6\pi\mu r_p)^2 + 2F_R\xi\rho s}\tanh\left(\frac{1}{2m}\left(t\sqrt{(6\pi\mu r_p)^2 + 2F_R\xi\rho s} + 2m\operatorname{arctanh}\left(\frac{6\pi\mu r_p}{\sqrt{(6\pi\mu r_p)^2 + 2F_R\xi\rho s}}\right)\right)\right)\right) \tag{17}$$

In this study, we obtained the impact velocity of the micro-abrasive particle, and based on the Hertz contact theory, the impact pressure of the micro-abrasive particle (P_p) in the medium water can be derived (Eq. (18)).

$$P_P = \frac{1}{3}\left(\frac{5}{4}\rho_p\right)^{\frac{3}{5}}\left[\pi\left(\frac{1-v_p^2}{E_p}+\frac{1-v_w^2}{E_w}\right)\right]^{-\frac{2}{5}} V_P^{\frac{6}{5}} \tag{18}$$

where ρ_p is the density of SiO_2, v_p and v_w are the Poisson ratio of the micro-abrasive particle and water, respectively, and E_p and E_w are the elastic moduli of the micro-abrasive particle and the bulk modulus of water, respectively. In the calculations, $\rho_p = 2200\ \mathrm{kg/m^3}$, $v_p = 0.2$, $v_w = 0.5$, $E_p = 69$ GPa, and $E_w = 2.18$ GPa. The continuous governing equations of the shock wave, micro-jet and micro-abrasive particle affected by the dimensionless amount of collapse of cavitation bubbles are as follows:

$$\begin{cases} \left(1-\frac{\dot{R}}{c}\right)R\ddot{R}+\frac{3}{2}\dot{R}^2\left(1-\frac{\dot{R}}{3c}\right)=\frac{P}{\rho}+\frac{1}{\rho c}\frac{d}{dt}(RP)=\left(1+\frac{\dot{R}}{c}\right)\frac{P}{\rho}+\frac{R}{\rho c}\frac{dP}{dt} \\ P_s = c_1\rho u_s\left(10^{(u_s-c)/c_2}-1\right)+P_\infty \\ u_s = c + c_2 \lg\left(\frac{\dot{R}}{c_1}+1\right) \\ V_j = 8.97\left(\frac{H}{R_0}\right)^2\sqrt{\frac{P_\infty - P_v}{\rho}} \\ P \approx V_j\rho_0 c_0 \\ V_P = \frac{1}{\xi\rho s}\left(-6\pi\mu r_p+\sqrt{(6\pi\mu r_p)^2+2F_R\xi\rho s}\tanh\left(\frac{1}{2m}\left(t\sqrt{(6\pi\mu r_p)^2+2F_R\xi\rho s}+2m\,\mathrm{arctanh}\left(\frac{6\pi\mu r_p}{\sqrt{(6\pi\mu r_p)^2+2F_R\xi\rho s}}\right)\right)\right)\right) \\ P_P = \frac{1}{3}\left(\frac{5}{4}\rho_p\right)^{\frac{3}{5}}\left[\pi\left(\frac{1-v_p^2}{E_p}+\frac{1-v_w^2}{E_w}\right)\right]^{-\frac{2}{5}} V_P^{\frac{6}{5}} \end{cases} \tag{19}$$

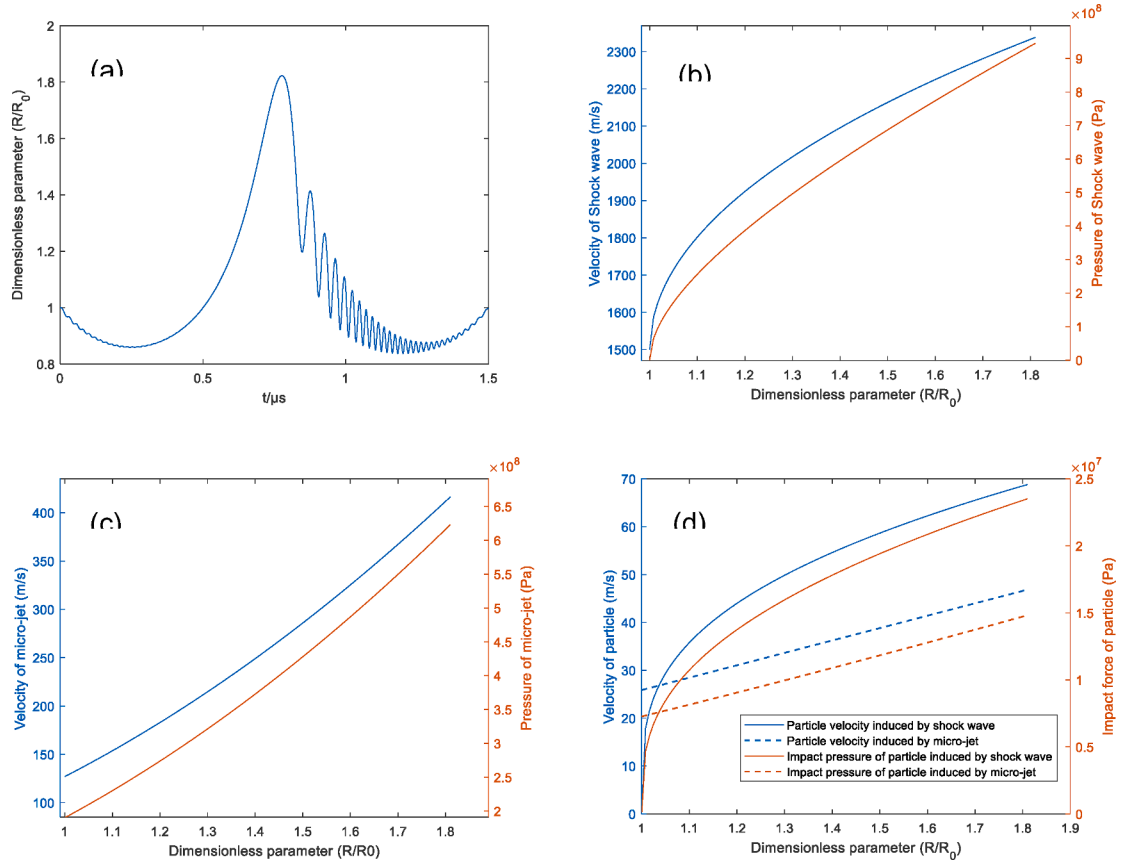

Fig. 2. Numerical simulation results obtained according to the initial environmental conditions in Table 1. (a) Simulation result of bubble oscillation; (b) and (c) simulation results of the velocity–pressure of the shock wave and the micro-jet, respectively, concerning the dimensionless amount of bubble collapse; (d) particle velocity and impact pressure results induced by the shock wave and the micro-jet.

3. Results and discussion

All images in Fig. 2 were obtained by numerical simulation according to the initial environmental conditions in Table 1. Fig. 2(a) shows a schematic diagram of cavitation bubble oscillation with time in one cycle. According to the cavitation bubble dynamics of the cavitation bubble oscillating rupture, the radius of the first oscillating rebound of the cavitation bubble is extracted and used as the collapse radius. Fig. 2 (a) shows that the dimensionless amount (R/R_0) range of bubble collapse is 1–1.81. Numerical analysis of the shock wave model, micro-jet model, and micro-abrasive particle model was conducted by the dimensionless amount (R/R_0) range of cavitation bubble collapse.

In Fig. 2(b) and (c), the velocity and pressure, respectively, of the shock wave in the initial environment are plotted. In Fig. 2(b), the shock wave velocity and the pressure both increase in a semi-convex shape with increase in R/R_0. Numerical simulations revealed that the initial speed of the shock wave was supersonic, the shock wave simulation speed was 1500–2338 m/s, and the maximum shock wave pressure was 945 MPa. Fig. 2(c) shows that the micro-jet velocity and pressure increase in a semi-convex shape with increase in R/R_0. The velocity range of the micro-jet is 127.1–416.3 m/s, and the maximum pressure range is 190.2–623 MPa. The experimental or numerical simulation data of some researchers on the velocity and pressure of the shock wave and micro-jet are presented in Tables 2 and 3, respectively. We conducted numerical simulations to compare with Tables 2 and 3 and found our model to be reasonable, valid, and valuable.

The behavior of the micro-abrasive particles is simulated in Fig. 2(d); the appropriate abrasive particle size should be selected. First, when one side of the bubble was in initial contact with the particle, the particle velocity was smaller than the surface velocity of the bubble, which caused a flat shape similar to the interaction between the bubble and the rigid wall [44], forming a micro-jet to act on the particle. Therefore, in the selection of abrasive particle parameters, it is first considered that the cavitation micro-jet will not cause large-scale abrasive particle breakage, reducing the energy loss of the cavitation micro-jet acting on the abrasive particles and ensure that more energy is transmitted with increasing kinetic energy of the abrasive particles. Second, Borkent et al. [45] demonstrated that the viscous resistance on micron-sized particles is negligible during the first cycle of the bubble. Thus, if the particle size is small and the concentration is low, it is captured by the center of the micro-jet and they move together. A rougher the particle surface promotes the formation of cavitation nucleation. Borkent [46] verified the influence of different types of particles on cavitation events and concluded that surface roughness and hydrophobicity of particles are important factors affecting cavitation activity; the cavitation activity of rough surface particles and hydrophobic particles is stronger. Arora [47] experimentally observed smooth surface particles without cavitation even at very high stress levels.

Thus, to avoid the crushing of abrasive particles, reduce the influence of cavitation nucleation, and consider the existence of viscous resistance, we selected smooth spherical SiO_2 particles with an abrasive particle radius of 10 μm for initial numerical simulation.

In Fig. 2(d), numerical simulation results show that the maximum velocity and maximum pressure of 10 μm smooth spherical SiO_2 particle induced by the force of shock wave and micro-jet, respectively, are 68.8 m/s, 46.85 m/s and 23.51 MPa, 14.82 MPa, respectively, for R/R_0 range of 1–1.81. Both curves show an increasing trend; especially, the velocity of the micro-abrasive particle subjected to the force of the micro-jet does not start from zero, which again proves that the shock wave is generated before the micro-jet and that the residual shock wave gives the micro-abrasive particle a certain velocity. Based on previous investigations, as shown in Table 4, the simulated velocities of the micro-abrasive particles modeled in this study are in general agreement with the simulated range of particle velocities and the actual range of processing under general environmental conditions. The impact pressure of a particle is obtained based on the velocity, and the correctness of the particle size-velocity model of micro-abrasive particles also verifies the impact pressure model of the particles.This is sufficient to show that the proposed research is correct and valuable, and suitable for further in-depth exploration and analysis. However, the abrasive particle velocity is greatly affected by particle size, viscosity, and concentration of the liquid medium. Changes in any condition will significantly alter the abrasive particle velocity. The effect of particle size on particle velocity and impact pressure are described next in Section 3.3.

We set different ultrasonic frequencies, pressure amplitudes and particle sizes to investigate their effects on the velocity and pressure of shock waves, micro-jets, and micro-abrasive particles. The value of R/R_0 of the cavitation bubble changed considerably by the above factors. Specific impacts are presented in Sections 3.1, 3.2 and 3.3.

Table 4
Examples of micro-abrasive particle velocities.

Literature	Cavitation source	Method of derivation	Particle diameter	Particle velocity
Prozorov [28]	Ultrasound (20 kHz)	Numerical&SEM	2.2–38 μm	750–3250 m/s
Tan [29]	Ultrasound	Numerical&HSC	5–50 μm	8–40 m/s
Borkent [45]	Tensile stress wave	Experimental	68 μm	37 m/s
Doktycz [48]	Ultrasound (20 kHz)	Experimental calculations	10 μm	100–500 m/s

3.1. Effects of ultrasonic field-frequency

The frequency of the ultrasonic field is an important factor affecting cavitation. In the range of 20–100 kHz, we selected the ultrasonic frequencies of 20 kHz, 60 kHz, and 100 kHz for simulation and determined the most suitable frequency for ultrasonic processing. The test results are shown in Fig. 3.

As shown in Fig. 3, at an ultrasonic frequency of 20 kHz, the oscillation of cavitation bubble is the most regular; compared with the ultrasonic frequencies of 60 kHz and 100 kHz, the dimensionless amount can reach the maximum value at 20 kHz. At ultrasonic frequencies of 60 kHz and 100 kHz, the period of cavitation bubble collapse is shorter and R/R_0 is smaller than that at an ultrasonic frequency of 20 kHz. There is an irregular cavitation bubble oscillation curve, which is not conducive to precision ultrasonic machining. In ultrasonic-assisted machining, regular cavitation oscillation is selected, which is conducive to the control of cavitation effect and can also improve machining accuracy. As shown in the simulation results, in the range of 20–100 kHz, the

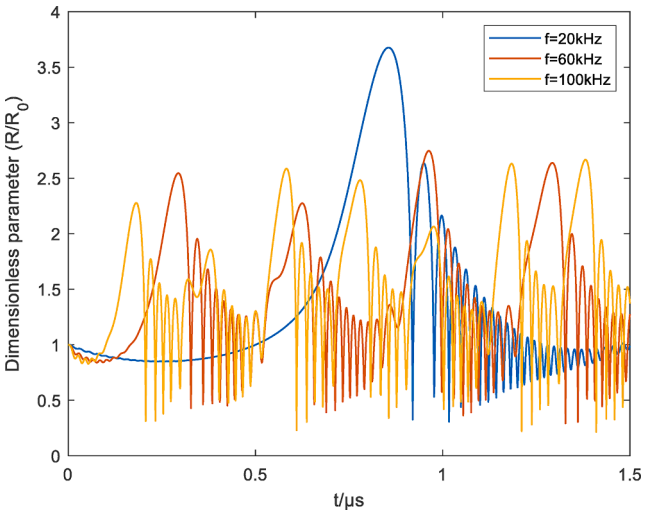

Fig. 3. Simulation results for different ultrasound frequencies.

ultrasonic frequency of 20 kHz is the most suitable for ultrasonic processing under the current conditions. This is also consistent with the experimental conditions of several studies [28,48].

3.2. Effects of ultrasonic field-sound pressure

The sound pressure amplitude of the ultrasonic field is another important factor that affects cavitation. For a cavitation bubble with an initial radius, $R_0 = 0.5$ μm, the cavitation threshold is approximately 0.1125 MPa, calculated according to the cavitation threshold formula. Three different sound pressure amplitudes are set, namely, 0.0375 MPa, 0.075 MPa, and 0.1125 MPa, to study the cavitation oscillation, as shown in Fig. 4:

As shown in Fig. 4, in the range of cavitation threshold of 0.1125 MPa, $R/R_0 \in [1,3.676]$, the velocity range of shock wave is 1500–2980 m/s, and the maximum pressure generated is up to 2189 MPa; The velocity range of micro-jet is 134 ~ 1717 m/s, and the generated pressure can reach 2570 MPa. According to the numerical values, greater amplitude of the sound pressure implies greater maximum value of R/R_0, more violent oscillation of the cavitation bubble, and a more obvious cavitation effect. Therefore, to improve the processing efficiency, obtain cavitation bubbles with greater energy, and produce more effective cavitation effects, a sound pressure amplitude close to the threshold for processing within the cavitation threshold range should be selected. In practice, however, accurately controlling the sound pressure amplitude in ultrasonic machining is challenging; this problem should be investigated more in the future.

3.3. Effects of micro-abrasive particle

The kinetic energy of abrasive particles is related to particle size and velocity at the same time, and we aim to obtain the optimal solution for abrasive particle size and velocity. For the simulation conditions, we selected the ultrasonic sound pressure amplitude of 0.1125 MPa according to the discussion presented in section 3.2. A micro-abrasive particle with a very small size (especially when the radius of the micro-abrasive particle is smaller than that of the cavitation bubble, under the conditions of this study, it is < 5 μm) is sucked into the center of the micro-jet and moves together with it; for a micro-abrasive particle with a very large size ((under the conditions of this study, > 50 μm), due to the tiny size of the bubbles, the abrasive grains do not have a significant velocity. Therefore, under the conditions of this study, the radius of the abrasive particles is in the range of 5–50 μm, and a realistic moving velocity can be obtained. Therefore, smooth spherical SiO_2 particles with radii of 5 μm, 10 μm, 20 μm, 30 μm, 40 μm, and 50 μm were selected. The simulation results for different particle size velocities are shown in Fig. 5.

As shown in Fig. 5, smooth spherical SiO_2 particles of six different radii (5 μm, 10 μm, 20 μm, 30 μm, 40 μm, and 50 μm) were subjected to shock wave force-induced and micro-jet force-induced particle velocity and pressure when the cavitation bubble collapsed to the maximum dimensionless level. As shown in Fig. 5(a), the particle velocities induced by the dominant shock wave force induced were 209.4 m/s, 104.7 m/s, 52.36 m/s, 34.91 m/s, 26.18 m/s, and 20.94 m/s; (b) the particle velocities induced by the dominant micro-jet force induced were 190.3 m/s, 95.15 m/s, 47.57 m/s, 31.72 m/s, 23.79 m/s and 19.03 m/s; (c) pressures induced by shock wave were 5.641 MPa, 7.373 MPa, 10.41 MPa, 16.94 MPa, 38.92 MPa, and 89.41 MPa; and (d) pressures induced by the micro-jet were 5.028 MPa, 6.572 MPa, 9.281 MPa, 15.1 MPa, 34.69 MPa, and 79.69 MPa, respectively.

As shown in the results, whether it is micro-abrasive particle movement induced by the force of shock wave or micro-jet, the effects of particle size on velocity and pressure are intuitive and clear. Larger dimensionless amount (R/R_0) results in greater velocity and pressure that the particle can obtain; larger particle size results in smaller velocity and pressure that the particle can obtain; As shown in Fig. 5, the increase in the velocity and pressure of the micro-abrasive particle increases with decreases in particle size; in particular, the velocity and pressure of the micro-abrasive particle increase by twice as particle size changes from 10 μm to 5 μm. When particle size decreases from 50 μm to 20 μm, the velocity and pressure of the micro-abrasive particle induced by the force of shock wave and micro-jet change only slightly. Under the conditions of this study, the maximum particle velocity and pressure, 209.4 m/s and 89.41 MPa respectively, can be obtained by selecting smooth spherical SiO_2 particles with a radius of 5 μm. the findings of this study provide insights for setting parameters for ultrasonic-assisted machining operations.

4. Conclusion

Quantification and control of shock waves and micro-jets in cavitation have been explored by several researchers. In the case of the micro-abrasive particles, most studies have analyzed particle velocities by inversion of the mass loss of the machined workpiece, however, in this study, the velocity of the micro-abrasive particle is directly modeled, providing insights for selecting ultrasonic parameters and micro-abrasive parameters in ultrasonic processing, reducing the cost of trials and errors. By controlling the changes of ultrasonic and abrasive parameters, numerical simulation analysis was carried out and following conclusions were obtained.

(1) The cavitation effect and the synergistic effect of micro-abrasives are mainly reflected in the fact that the shock wave promotes the formation of the micro-jet, the shock wave and the micro-jet give the micro-abrasive particle initial velocity, and the micro-abrasive particle that obtains a certain velocity in the actual machining must be able to promote the change of the surface shape of the workpiece. The synergistic effect of the three is far better than the effect of one or two alone. Based on the theoretical basis of shock waves and micro-jets in cavitation bubbles and cavitation effects, the continuous governing equations of shock wave, micro-jet and micro-abrasive particle affected by the dimensionless amount of collapse of cavitation bubble are established. Analysis results show that the ultrasonic frequency of

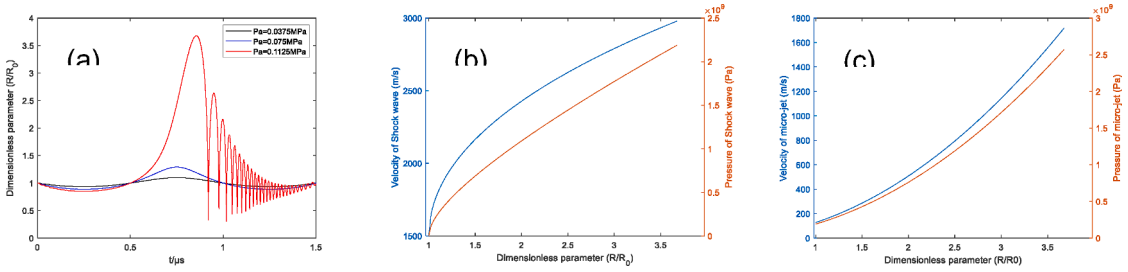

Fig. 4. Simulation results for different ultrasound sound pressure conditions. (a) Oscillation of the vacuole at sound pressure amplitude $P_a = 0.0375$ MP, 0.075 MPa and 0.1125 MPa; (b) and (c) simulation results of the velocity–pressure of the shock wave and micro-jet, respectively, for the maximum value of R/R_0.

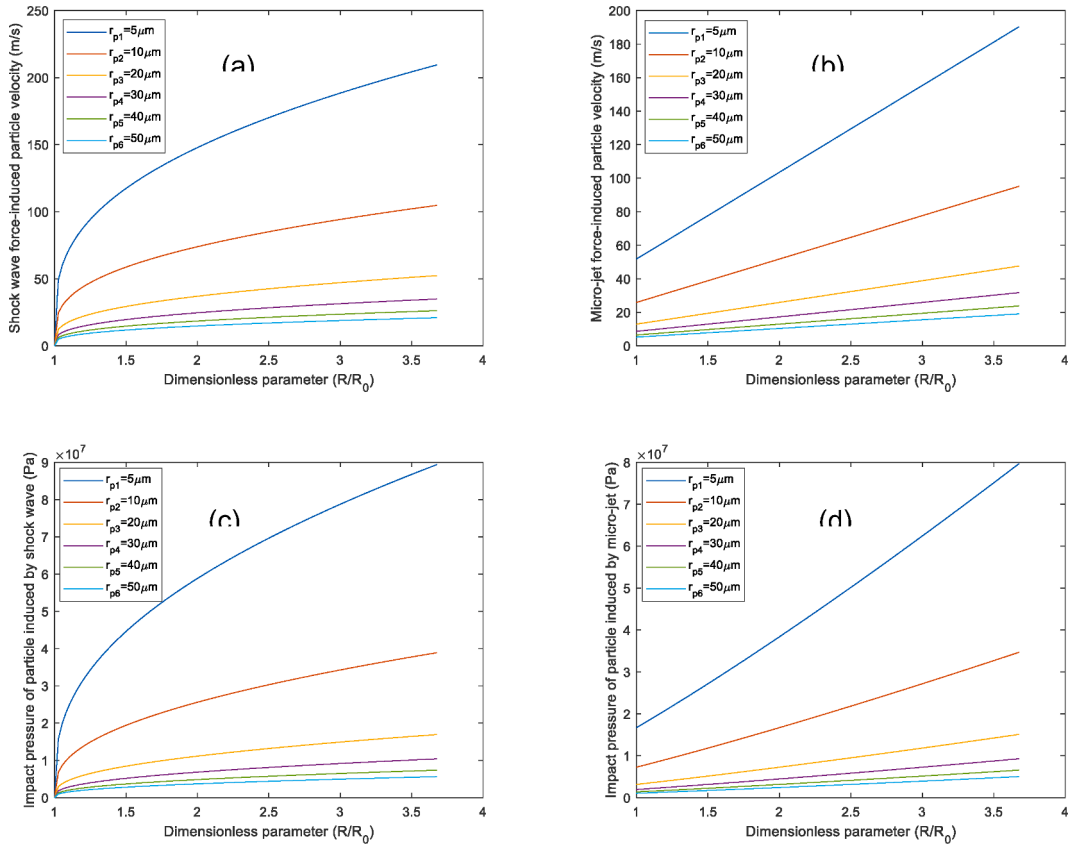

Fig. 5. (a) and (b) Particle size-velocity simulation results of the micro-abrasive particle induced by the force of shock wave and micro-jet, respectively. (c) and (d) Particle size-pressure simulation results of the micro-abrasive particle induced by the force of shock wave and micro-jet, respectively.

20 kHz and ultrasonic sound pressure of 0.1125 MPa can produce the largest dimensionless amount, $R/R_0 = 3.676$, of cavitation collapse.

(2) When the maximum dimensionless amount ($R/R_0 = 3.676$) is reached, the velocity and pressure of the shock wave and the micro-jet can both reach the maximum. Compared with the initial simulation condition when $R/R_0 = 1.81$, the shock wave velocity increased by 642 m/s and the pressure increased by 1244 MPa. The velocity and pressure of the micro-jet increased by more than four times. That is, larger dimensionless amount, implies greater shock wave, micro-jet velocity and pressure generated by the cavitation effect.

(3) The particle size-velocity–pressure model of micro-abrasive particle was established, and particle size was found to have a significant effect on velocity and pressure. Selecting 5–50 μm micro-abrasive particles with sizes of 5–50 μm, the velocity range was 19.03–209.4 m/s, and the pressure range was 5.028–89.41 MPa. The maximum velocity and pressure of the micro-abrasive particle, whether induced by shock wave force or micro-jet force, were obtained at 5 μm. In the size range of 5–50 μm, smaller particle size of the micro-abrasive particles, implies that greater velocity and pressure can be obtained.

CRediT authorship contribution statement

Yingze Fu: Conceptualization, Methodology, Writing – original draft. **Xijing Zhu:** Supervision, Funding acquisition, Project administration. **Jianqing Wang:** Writing – review & editing. **Tai Gong:** Visualization, Investigation.

Declaration of Competing Interest

The authors declare that they have no known competing financial interests or personal relationships that could have appeared to influence the work reported in this paper.

Acknowledgment

This work has been supported by the National Natural Science Foundation of China (grant no. 51975540, 52005455).

References

[1] M. Ashokkumar, The characterization of acoustic cavitation bubbles – An overview, Ultrason. Sonochem. 18 (4) (2011) 864–872.
[2] Suslick, K.S., Sonochemistry. Science (New York, N.Y.), 1990. 247(4949): p. 1439-45.
[3] Lauterborn, W. and A. Vogel, Shock Wave Emission by Laser Generated Bubbles, in Bubble Dynamics and Shock Waves, C.F. Delale, Editor. 2013, Springer Berlin Heidelberg: Berlin, Heidelberg. pp. 67–103.
[4] O. Supponen, et al., Shock waves from nonspherical cavitation bubbles, Phys. Rev. Fluids 2 (9) (2017) 20.
[5] S.L. Xu, et al., Fabrication of hybrid micro/nano-textured surfaces using rotary ultrasonic machining with one-point diamond tool, Int. J. Mach. Tools Manuf 86 (2014) 12–17.
[6] S.L. Xu, et al., Development of a novel 2D rotary ultrasonic texturing technique for fabricating tailored structures, Int. J. Adv. Manuf. Technol. 89 (1–4) (2017) 1161–1172.
[7] H.S. Chen, et al., Damages on steel surface at the incubation stage of the vibration cavitation erosion in water, Wear 265 (5–6) (2008) 692–698.
[8] T. Okada, et al., Relation between impact load and the damage produced by cavitation bubble collapse, Wear 184 (2) (1995) 231–239.
[9] E.A. Brujan, et al., The final stage of the collapse of a cloud of bubbles close to a rigid boundary, Ultrason. Sonochem. 18 (1) (2011) 59–64.
[10] A. Vogel, S. Busch, U. Parlitz, Shock wave emission and cavitation bubble generation by picosecond and nanosecond optical breakdown in water, J. Acoust. Soc. Am. 100 (1) (1998).

[11] M. Kornfeld, L. Suvorov, On the Destructive Action of Cavitation, J. Appl. Phys. 15 (6) (1944) 495–506.
[12] L.Z. Ye, X.J. Zhu, Analysis of the effect of impact of near-wall acoustic bubble collapse micro-jet on Al 1060, Ultrason. Sonochem. 36 (2017) 507–516.
[13] N.K. Bourne, J.E. Field, Shock-induced collapse of single cavities in liquids, J. Fluid Mech. 244 (1992) 225–240.
[14] J.P. Dear, J.E. Field, A.J. Walton, Gas compression and jet formation in cavities collapsed by a shock wave, Nature 332 (1988).
[15] E. Klaseboer, et al., Interaction of lithotripter shockwaves with single inertial cavitation bubbles, J. Fluid Mech. 593 (2007) 33–56.
[16] M. Petkovsek, M. Hocevar, M. Dular, Visualization and measurements of shock waves in cavitating flow, Exp. Therm Fluid Sci. 119 (2020).
[17] M. Khavari, et al., Characterization of shock waves in power ultrasound, J. Fluid Mech. 915 (2021) 14.
[18] K. Johansen, J.H. Song, P. Prentice, Performance characterisation of a passive cavitation detector optimised for subharmonic periodic shock waves from acoustic cavitation in MHz and sub- MHz ultrasound, Ultrason. Sonochem. 43 (2018) 146–155.
[19] Pecha and Gompf, Microimplosions: cavitation collapse and shock wave emission on a nanosecond time scale, Phys. Rev. Lett. 84 (6) (2000) 1328–1330.
[20] E.A. Brujan, T. Ikeda, Y. Matsumoto, On the pressure of cavitation bubbles, Exp. Therm Fluid Sci. 32 (5) (2008) 1188–1191.
[21] R. Petkovsek, J. Mozina, G. Mocnik, Optodynamic characterization of shock waves after laser-induced breakdown in water, Opt. Express 13 (11) (2005) 4107–4112.
[22] Parlitz, A.V.A.S.B.A.U., Shock wave emission and cavitation bubble generation by picosecond and nanosecond optical breakdown in water. The Journal of the Acoustical Society of America%J, 1996. 100(1): pp. 148–165.
[23] W.K. Soh, B. Willis, A flow visualization study on the movements of solid particles propelled by a collapsing cavitation bubble, Exp. Therm Fluid Sci. 27 (5) (2003) 537–544.
[24] T.Q. Zhang, et al., Experimental and simulation studies of abrasive particles impacting monocrystalline silicon in suspension thin film flow field of ultrasonic polishing, Int. J. Adv. Manuf. Technol. 103 (1–4) (2019) 819–840.
[25] Ductile-regime grinding. A new technology for machining brittle materials: T. G. Bifano, T. A. Dow, R. O. Scattergood, Journal of Engineering for Industry, Transactions of the ASME, 113(2), pp. 184–189. (May 1991). Precision Engineering, 1992. 14(1): p. 54.
[26] C. Peng, et al., Erosion characteristics and failure mechanism of reservoir rocks under the synergistic effect of ultrasonic cavitation and micro-abrasives, Adv. Powder Technol. 32 (11) (2021) 4391–4407.
[27] L. Zhang, V. Belova, H. Wang, Controlled Cavitation at Nano/Microparticle Surfaces. Chemistry of Materials, 26, A Publication of the American Chemistry Society, 2014.
[28] T. Prozorov, R. Prozorov, K.S. Suslick, High velocity interparticle collisions driven by ultrasound, J. Am. Chem. Soc. 126 (43) (2004) 13890–13891.
[29] K.L. Tan, S.H. Yeo, Velocity estimation of micro-particles driven by cavitation bubble collapses through controlled erosion experiments, Int. J. Multiph. Flow 127 (2020) 8.
[30] Z.W. Liu, et al., Role of a nanoparticle on ultrasonic cavitation in nanofluids, Micro & Nano Lett. 14 (10) (2019) 1041–1045.
[31] M.S. Plesset, The dynamics of cavitation bubbles, J. Appl. Mech. 16 (3) (2021) 277–282.
[32] A., p.,, Bubble phenomena in sound fields: part one, Ultrasonics 22 (2) (1984).
[33] S. Behnia, et al., Towards classification of the bifurcation structure of a spherical cavitation bubble, Ultrasonics 49 (8) (2009) 605–610.
[34] E. Zilonova, M. Solovchuk, T.W.H. Sheu, Bubble dynamics in viscoelastic soft tissue in high-intensity focal ultrasound thermal therapy, Ultrason. Sonochem. 40 (2018) 900–911.
[35] M.H. Rice, J.M. Walsh, Equation of state of water to 250 kilobars, J. Chem. Phys. 26 (4) (1957).
[36] S.W. Ohl, E. Klaseboer, B.C. Khoo, Bubbles with shock waves and ultrasound: a review, Interface Focus 5 (5) (2015) 15.
[37] S., P.M. and C.R. B., Collapse of an initially spherical vapour cavity in the neighbourhood of a solid boundary. Journal of Fluid Mechanics, 1971. 47(2).
[38] J. Holzfuss, Acoustic energy radiated by nonlinear spherical oscillations of strongly driven bubbles, Proc. R. Soc. A Mathemat. Phys. Eng. Sci. 466 (2118) (2010) 1829–1847.
[39] I. Tzanakis, et al., Incubation pit analysis and calculation of the hydrodynamic impact pressure from the implosion of an acoustic cavitation bubble, Ultrason. Sonochem. 21 (2) (2014) 866–878.
[40] L.Z. Ye, et al., Ultrasonic cavitation damage characteristics of materials and a prediction model of cavitation impact load based on size effect, Ultrason. Sonochem. 66 (2020) 6.
[41] Y.A. Pishchalnikov, et al., High-speed video microscopy and numerical modeling of bubble dynamics near a surface of urinary stone, J. Acoust. Soc. Am. 146 (1) (2019) 516–531.
[42] R. Petkovsek, P. Gregorcic, A laser probe measurement of cavitation bubble dynamics improved by shock wave detection and compared to shadow photography, J. Appl. Phys. 102 (4) (2007) 9.
[43] H.S. Chen, et al., Effect of hydrodynamic pressures near solid surfaces in the incubation stage of cavitation erosion, Proc. Inst. Mech. Eng. Part J-J. Eng. Tribol. 222 (J4) (2008) 523–531.
[44] Ea., b.,, et al., The final stage of the collapse of a cavitation bubble close to a rigid boundary, Phys. Fluids 14 (1) (2002).
[45] B.M. Borkent, et al., The acceleration of solid particles subjected to cavitation nucleation, J. Fluid Mech. 610 (2008) 157–182.
[46] B.M. Borkent, M. Arora, C.D. Ohl, Reproducible cavitation activity in water-particle suspensions, J. Acoust. Soc. Am. 121 (3) (2007) 1406–1412.
[47] M. Arora, C.-D. Ohl, K.A. Morch, Cavitation inception on microparticles: a self-propelled particle accelerator, Phys. Rev. Lett. 92 (17) (2004), 174501.
[48] S.J. Doktycz, K.S. Suslick, Interparticle collisions driven by ultrasound, Science (New York, N.Y.) 247 (4946) (1990) 1067–1069.